Post-print version of:

Title: **Automated Experimental Modal Analysis of Bladed Wheels with an Anthropomorphic Robotic Station**

Authors: **L. Bertini, P. Neri, C. Santus, A. Guglielmo**

Automated experimental modal analysis of bladed wheels with an anthropomorphic robotic station

Leonardo Bertini · **Paolo Neri** · **Ciro Santus** ·

Alberto Guglielmo

Abstract Experimental modal analysis is challenging when the component has a highly three-dimensional shape, since a great number of measurement points are needed with accurate positioning. An anthropomorphic robotic station is proposed to automate this analysis, specifically on bladed wheels. This provides a reliable control of the spot location and of the beam orientation of a Laser Doppler Vibrometer. The modal frequencies were obtained along with the vibrational shapes and their spatial resolution was managed by exploiting the programming flexibility of the robotic station. The SAFE diagram was easily obtained by measuring a single point for each sector, and an extension of this diagram was demonstrated for the splitter blade wheels. The use of multiple measurement points, for each wheel sector, significantly improved the characterization of the modes having the same number of nodal diameters, hence the same shape coordinate on the SAFE diagram.

L. Bertini · P. Neri (✉) · C. Santus

University of Pisa. Department of Civil and Industrial Engineering, Mechanical division. Largo L. Lazzarino 1, 56122 Pisa, Italy

E-mail: leonardo.bertini@ing.unipi.it paolo.neri@dici.unipi.it ciro.santus@ing.unipi.it

A. Guglielmo

General Electric, Oil & Gas. Nuovo Pignone. Via Felice Matteucci 2, 50127 Florence, Italy

E-mail: alberto.guglielmo@ge.com

1 Introduction

Industrial product development today entails optimizing the design and continuously enhancing performance. This forces the designer to carefully consider all the possible failure mechanisms in order to improve the in-service performance. A great effort is made in preventing catastrophic failures during the operational conditions, as proved by the damage monitoring techniques described in the literature [1–8]. An accurate dynamic characterization of any mechanical component, that experiences cyclic loadings, is needed to estimate its behavior under operational conditions. Analytical and numerical analyses are clearly useful at the design stage, however experimental tests are always recommended for very complex component geometries or large assemblies. Highly three-dimensional structures need a large number of measurement points to be able to obtain the modal shapes. The accelerometer testing approach was not considered feasible for this application, since many sensors would be needed which would be time consuming and also affect the mechanical response of the component. The cumbersome work of accelerometer monitoring can be circumvented by measuring with contactless solutions either the vibrational displacement, with high speed cameras [9], or the speed with a Laser Doppler Vibrometer (LDV) [10]. Of these two measurement techniques, LDV provides the highest frequency range. Scanning Laser Doppler Vibrometry (SLDV) is often adopted for the dynamic analysis of bladed wheels, and some examples are provided by [11–15]. Altough SLDV scans wide areas by being able to position the laser spot without moving the sensor head, no control is available for the beam direction. This implies that the angle between the laser beam and the surface normal cannot be arbitrarily chosen, those reducing signal quality and measurement degrees of freedom, especially for highly three-dimensional geometries. Moreover, if the sensor head is in a fixed position, obstacles may be encountered by the laser beam when pointing at a target. Finally, no positioning feedback is available during the measurements, thus unexpected position errors may occur [16]. To avoid these issues, standard LDV measurements were preferred with a single point sensor head moved step by step to each measurement location. Manual positioning and orientation of the laser device can still lead to long and defective tests. As suggested by the authors [17], and similarly to the automotive industry application RoboVib by Polytec [18], the handling issues could be solved by a robotic station, hence obtaining a stable configuration during the measurements, good accuracy, high resolution and also fast positioning. Bertini et al. [17] used an ABB anthropomorphic arm to guide an LDV sensor head and, after the initial alignment operation, a precise relative positioning was achieved in a reasonable time. The capabilities of this Robot-LDV technique are well matched for bladed wheels, and given the complex geometry, all the six degrees of freedom of an anthropomorphic robotic arm are needed. The cyclic feature of these wheels requires the

corresponding measurement points at each sector, thus high accuracy in terms of both positioning and orientation are crucial. The automation and the flexibility provided by the robotic station facilitated an industrial approach, and the test could be easily reprogrammed for different wheel types or sizes, instead of being forced to set up a new procedure for any newly introduced article.

It is worth noting that a hybrid solution could be optimal: an SLDV sensor head could be mounted on the robotic arm and then positioned in front of each blade to ensure a proper beam orientation. The blade surface could then be scanned without having to re-position the robotic arm, thus further reducing the measurement time also for a great number of points on each blade. In the present application, the duration of the whole test was further reduced by implementing an automatic procedure throughout the modal analysis. The LMS hardware and software enabled an interface with an external programming code, such as Visual Basic, to drive all the test sequences: positioning, excitation, measurements and data storing. After the test, the data saved were processed to extract the modal results: eigenvalues, eigenvectors and dumping factors. In the present study the robotic station was used to test two different centrifugal compressor bladed wheels, one shrouded and the other unshrouded. The unshrouded wheel had the splitter blade feature, which has some advantages such as efficiency, flow distribution regularization, and noise reduction [19–23] but impairs the sector cyclic symmetry, as discussed below. The literature offers a great number of test procedures for bladed wheels. Kammerer and Abhari [24] presented an operational conditions test (Operational Modal Analysis, OMA) by applying the load through different fluid distortions to excite the various modes. A simple and effective test can be performed by applying a cyclic load to a bladed wheel under stationary conditions, using one or more shakers (Experimental Modal Analysis, EMA) as in Bidaut and Baumann [10]. Although this approach apparently neglects the centrifugal effects, it still proves reliable since for this kind of structure the FE analysis showed a stress stiffening lower than 1% in terms of natural frequencies up to 10 000 rpm. A compromise between OMA and EMA can be achieved by testing a stationary wheel under a complex load field. Indeed, the well known SAFE diagram (Singh's Advanced Frequency Evaluation) as reported by Bloch and Singh [25], and recently analytically reconsidered by Bertini et al. [26], proved that a particular spatial force distribution is needed to properly energize each blade mode. This can be achieved by applying an excitation source, such as a shaker or an electromagnetic device, on each blade and controlling both the amplitude and the phase of each applied force, as shown in the experiment by Berruti et al. [27]. The complexity of these tests is justified when higher frequency modes are studied and operational conditions need to be simulated. On the other end if lower frequency modes are studied, which are usually the most dangerous, a single-input to multiple-output test is sufficiently accurate. The present paper shows this latter kind of test. An electrodynamic shaker was chosen as the

excitation source which was mounted onto the structure through a stinger and a load cell. This contact technique has some disadvantages, as pointed out by several researchers who developed contactless excitation solutions based on either acoustic devices citever, laser pulses [28], pressurized air [29,30], or magnetic fields [12]. The need to directly attach the shaker to the structure is questionable in the present application since it could influence the cyclic symmetry of the component, thus influencing its dynamic response [12]. The available contactless solutions have other drawbacks. They generally provide weak forces (low signal-to-noise ratio) and a small operational frequency range. Furthermore, contactless solutions present severe difficulties in measuring the applied force, thus leading to possible FRF estimation errors. Conversely, standard shakers provide high forces, wide frequency ranges, and the influence of the mounting on the structure can be drastically mitigated by using a suitable stinger [31,32].

The vibration response was measured at different blade positions for the investigated wheels. The use of many measurement points for each sector of the wheel emphasized the method's effectiveness and the accuracy of the results was confirmed after comparing the mode frequencies and the mode shapes to Finite Element (FE) results. FE modeling is usually recommended along with the experimental activity, when investigating these kinds of structure, for comparison purposes. Due to the component cyclic symmetry, only one sector could be modelled in order to reduce the number of elements, however, neglecting any mistuning. Several methods can be exploited to take into account mistuning within a FE analysis [11,33–35] but some experimental data are needed to calibrate these models. The experimental results confirmed that for the bladed wheels tested, mistuning slightly affects a few natural modes, above all introducing a separation between double modes.

2 Experimental set up

The component being tested was placed in the robot working volume and was excited by a controlled vibration source. The element tested was held by simulating the "free-free" boundary condition, which enabled the component itself to be analysed without being affected by the clamping equipment. More accurate comparisons between experimental and numerical results were obtained by following this approach, since uncertain boundary conditions are usually challenging to be properly simulated with a FE model. The free-free constraint condition is usually experimentally achieved by using low stiffness elastic supports, such as inflated inner tubes or elastic bands, which bear the weight of the component and minimize any action against the vibration [36]. The high mass of the structure, and the low stiffness of the inner tube support, produced very low frequency rigid body modes, thus leaving the higher frequency modes of the structure unchanged. More precisely, rigid body mode frequencies were found to be less than 0.3% of

the lowest deformation mode frequency. A negligible response interaction by the inner tube with the high frequency excitation is therefore expected, and consequently no relevant dumping is introduced by the support during tests. The cyclic load was applied with a TiraVib electrodynamic shaker: 18 N peak force, 20 kHz maximum frequency, with a load cell mounted on the shaker, and a stinger used to connect the actuator to the structure. The applied excitation was a white noise random signal, the frequency band overlapped the investigated mode range and the Hanning windowing was applied. The vibrational response was measured with a Laser Doppler Vibrometer (LDV) by Polytec providing a high sensitivity in a wide frequency range, up to 50 kHz. The sample frequency during the test was set to (approx.) 2.2 times the maximum excitation harmonic, in order to avoid aliasing. The sensor head can only measure the velocity component of the vibration aligned with the laser beam direction. Therefore, the measurement location needs to be spotted with the desired orientation (orthogonal to the blade surface) and also respecting the sensor stand-off distance requirements. An anthropomorphic robotic arm manufactured by ABB was used to ensure the correct laser positioning and orientation. Manual placing can take several minutes for each measurement point, and gives no feedback in terms of location precision. Conversely, the robotic station rapidly places the sensor with a known maximum error which is less than 1 mm in the whole working volume, and even less if the robot volume is partitioned, with a repeatability uncertainty less of 0.2 mm. Since the robot introduces this high positioning reliability, the measurements can be repeated at different times, thus offering high levels of versatility.

All LDV sensors have several discrete stand-off distances that give the maximum measurement signal power, thus the laser needs to be placed with an offset with respect to the component analysed. The mounting of the laser head on the robot wrist is thus crucial in order to maximize the actual measurement volume of the robotic station. A mounting with the laser beam orthogonal to the wrist Z axis was chosen, Fig. 1, as derived from the robotic welding torch configuration.

The test equipment also involved LMS hardware (SCADAS) and software (Test.LAB). The hardware enabled up to eight measurement channels to be acquired, providing two outputs for the control of the shakers, and the software included the data acquisition and the post-processing procedures. The user was also allowed to program a specific procedure which can interact with Test.LAB to automatize the test. The equipment is represented in Fig. 2 (a), which shows an example of laser positioning on a measurement location. The multiple measurement point pattern on each blade of the wheel is shown in Fig. 2 (b).
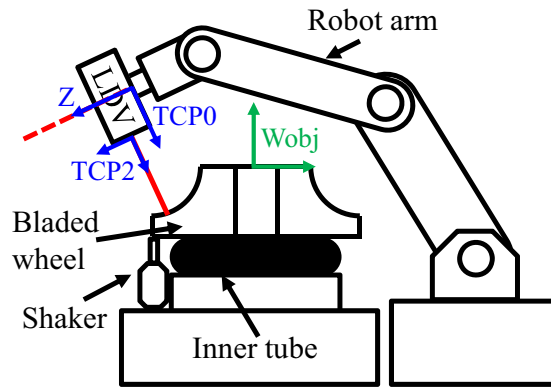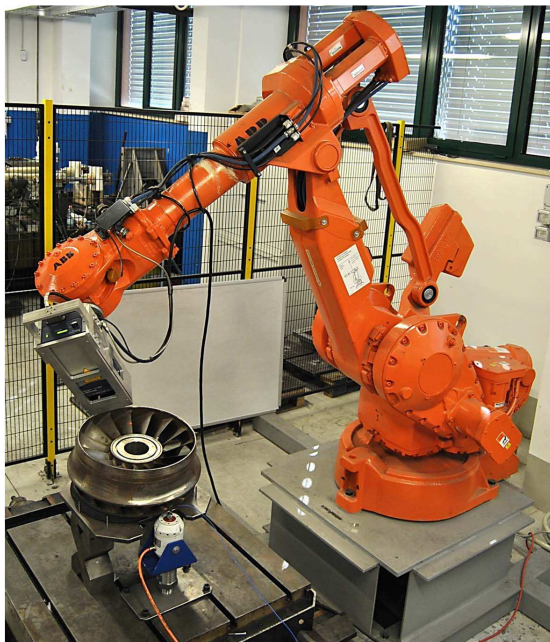
Fig. 1 Test set up, laser mounting solution and reference frames.

(a)   (b)

Fig. 2 (a) Robotic station and LDV positioning on the tested wheel, (b) indication of multiple measurement points on each blade.

2.1 Reference frame definition

As mentioned above, the laser spot positioning and orientation with respect to the component geometry is crucial for our application. The ABB robot was initially programmed to move with respect to a factory-defined reference frame, which is centred in the middle of its basement, and with a vertical Z axis. Another factory-defined reference frame is the wrist Tool Center Point (TCP0), which is placed on the centre of the wrist flange, Fig.1. Clearly, it is possible to create several alternative user-defined reference frames, which can be useful for programming. Those coordinate systems can be TCPs placed on relevant tool locations or Work objects (Wobj), which are usually centred on a significant location of the target object. Any movement instruction defines the final position and the

orientation of the chosen TCP with respect to the desired Wobj. For our application, a Wobj placed on the studied wheel and a TCP centred and aligned with the laser beam need to be defined. It is then possible to precisely place the laser spot by knowing the measurement locations and orientation from a CAD file of the analysed component. The robot embedded Wobj definition procedure requires a TCP to touch three points of the object in order to define the axes X, Y, Z. A sharp tip was mounted on the sensor-head protection cage and its vertex was used as a pointer. To define the TCP1, which is the one centred at the sharp tip, a fixed location P_0 in the workspace was chosen, and the TCP1 origin was manually positioned on that location with four different orientations. This procedure was very efficient when dealing with tangible tools, such as the sharp tip used to define the TCP1. However, the laser beam is not tangible and the laser spot location on a surface is not easy detect since the focused spot is much smaller than the naked eye reflected pattern. To overcome this, a webcam sensor (connected to a PC) was used to precisely locate the laser spot on a plane. This enabled the TCP2 to be defined, centred and aligned with the laser beam, by choosing a location P_1 on the sensor. The laser spot was then pointed at P_1 with four angular orientations. The distance between the laser head and P_1 was kept constant for each positioning. The TCP2 Z axis was easily defined by translating (and not rotating) the robot wrist, pointing the location P_1 at any distance. Finally, the precision of TCP2 Z axis definition increased when the chosen distance also increased.

2.2 Automatic testing procedure

When the reference frames have been defined, the robot can automatically move the sensor head to reach any desired target location and orientation. However, all the hardware and software involved in the measurement were integrated to obtain a fully automated testing procedure. Control software was developed to coordinate all the test components. Visual Basic (VB) was chosen as it was compatible with all the equipment involved as well as the technical support available for the LMS products. The data acquisition and the analysis was performed using LMS Test.Lab software. The measurement points and their orientation were obtained from the CAD model of the bladed wheel. These were initially stored in a Test.Lab project by providing a target list available for the robot. Other test set up information was required, such as the acquisition sampling frequency, the bandwidth range and the excitation intensity. The VB program was then used to import the geometry information from the project and to communicate the first target location to the robotic arm. After the robot completed its positioning task, the VB program received a feedback signal and the laser autofocus was started by sending a command string to the laser controller. When the laser was properly positioned and focused, the measurement was started. The Test.Lab switched on the excitation

source and also the acquisition channels, recording the force applied by the shaker and the vibrational velocity. Once the measurement was completed and the data stored, feedback was sent to the VB program, so that the procedure could be repeated for the other measurement points, as shown in the flow chart, Fig. 3.
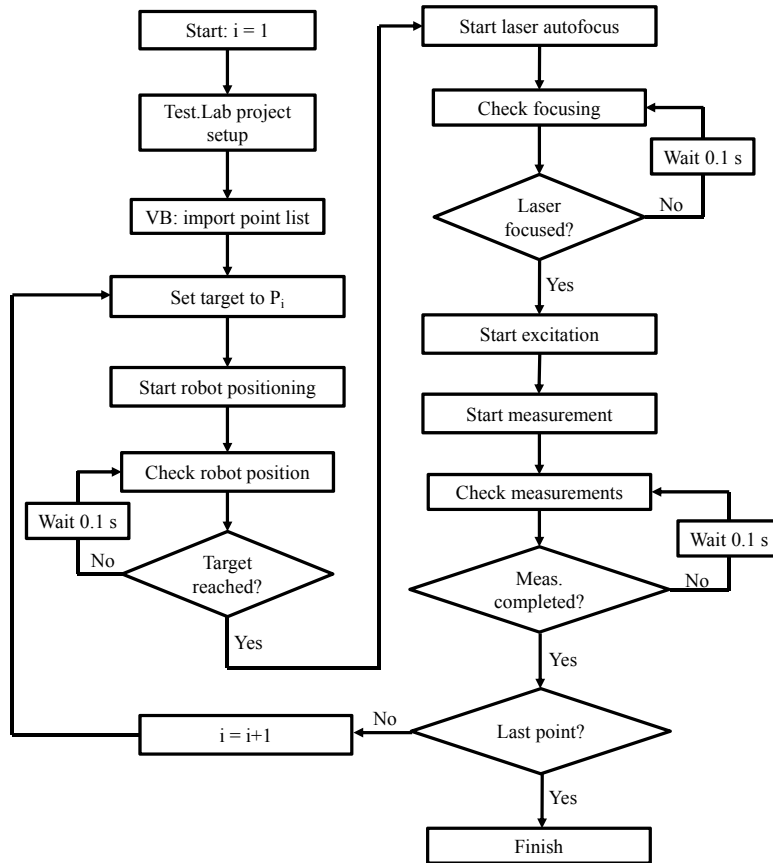
Fig. 3 VB program flow chart for implementing the overall testing procedure.

Two different strategies can be used to position the robot. The easiest one is to move the robot directly from one measurement location to the next. Though this solution is fast, as the spatial movement is reduced to a minimum, it is neither safe nor robust. This approach does not enable each positioning to be studied independently, but the whole measurement path must be considered and the target order becomes important. For example, two different locations (P_1 and P_2) may be both reachable for the robot if starting from a rest position. Location P_2 may not be reachable however when the robot starts from a particular joint configuration required for P_1. Moreover, the direct movement from location P_1 to location P_2 could cause the robot to hit the testing structure with the sensor head. These issues can be solved by carefully planning the measurement path, but this is time consuming and also unreliable because the whole path needs to be redefined and checked whenever a new target point is added. A more robust strategy is to define a rest position P_0. Then, instead of directly moving from P_1 to P_2, the longer path P_1 - P_0 - P_2 can

be used. In this latter scenario, each measurement location can be evaluated independently from the others, since only the round trip P_0 - P_i ($i = 1, 2, \ldots$) needs to be checked. Since the overall test duration is mainly influenced by the focusing and measuring time, while positioning requires relatively shorter times, the second and more robust strategy was preferred. The much shorter time needed to plan the test largely compensated for the small testing time increase. The overall testing process required from 60 to 120 seconds approximately for each measurement location, mainly depending on the test set up and the component geometry.

3 Experimental modal analysis

The robotic station described is suitable for various applications in experimental structural dynamics. Any component with a complex shape, requiring a large number of measurement points, can be efficiently tested in a relatively short time with our automatic procedure. Possible examples of suitable mechanical components for this kind of analysis are vehicle chassis, small hulls or brake disks. This robotic arm based modal analysis has been applied to bladed wheels designed for centrifugal compressors. These are complex three-dimensional components, which typically show many different modal shapes in a narrow frequency range, thus requiring several measurement points to fully describe the structural vibration.

3.1 Bladed wheel modal shapes

Bladed wheels have a cyclic symmetry geometry, thus the natural modes are not only periodic with respect to time but also with respect to the angular coordinate. The displacements $\delta_{mk}(t)$ associated with the corresponding points on each k-th sector for the m-th mode can be represented by the product of two harmonic terms. These harmonic components can be expressed using the complex exponential notation and then extracting the real part of the complex number obtained. The real value can be obtained by calculating the real part of the complex product, or alternatively extracting the real parts before calculating the product. The first of Eqs. 1 is usually referred to as the complex form, while the second is the real form.

$$\delta_{mk}(t) = A_m \operatorname{Re}\left(e^{i(d_m k \Delta \vartheta + \vartheta_m)} e^{i(\omega_m t + \phi_m)}\right)$$

(1)

$$\delta_{mk}(t) = A_m \operatorname{Re}\left(e^{i(d_m k \Delta \vartheta + \vartheta_m)}\right) \operatorname{Re}\left(e^{i(\omega_m t + \phi_m)}\right)$$

In Eq. 1 $\operatorname{Re}(z)$ is the real part of the complex number z, A_m represents the oscillation amplitude of the m-th mode, d_m is the Number of Nodal Diameters (NND) of the m-th mode, $\Delta \vartheta = 2\pi/N_B$ is the sector angle (with N_B the

number of blades), ω_m is the mode angular natural frequency, and finally ϑ_m and ϕ_m are generic angular and time

phases. A nodal diameter is the locus of the points that do not move in the mode shape, and is equal to the half of the

sign reversals of the displacement along the hoop coordinate. Altough a continuous body has an infinite number of

natural modes, it can be proved that NND is limited by $d_{\max} = \lfloor N_B/2 \rfloor$ (where $\lfloor x \rfloor$ is the "floor" function). Since the

wheel only has N_B sectors, any angular frequency higher then $d_{\max}$ cannot be represented by N_B points because of

the aliasing phenomenon. A dynamic interpretation of the two forms of Eqs. 1 can be proposed. The first represents

a stationary wave with respect to the geometry, while the second represents a rotating wave travelling on the cyclic

structure (Fig. 4) and the rotational direction is related to the sign attributed to the angular frequency ω_m.
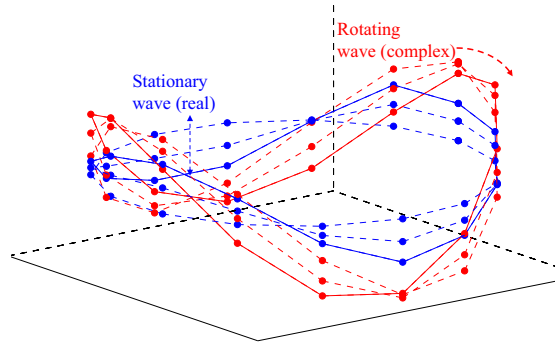
Fig. 4 Complex and real representation example of a mode with two nodal diameters.

Both these expressions are valid mode shape representations, since the stationary wave can be interpreted as the sum

of two counter-rotating waves. In cyclic symmetric FE analysis, each natural mode with a nonzero NND appears

as a couple of double modes with the same natural frequency. Both these modes represent the modal shape for that

particular natural frequency, as well as any linear combination of them. However, the regular shape of the modes

according to Eq. 1, is never reproduced experimentally since it is difficult to obtain the rotating waves from the

vibrational speed measurements. Indeed, only an almost perfectly tuned bladed wheel can return the rotating shape,

since in this situation the two coupled modes have exactly the same frequency, so that they can be combined as a

travelling wave. If any even small mistuning affects the bladed wheel structure, the two coupled modes have slightly

different frequencies. They are thus usually found as two distinct stationary modes, instead of two counter-rotating

waves, thus just the second of Eqs. 1 (the real form) applies and it is the only one considered hereafter. This equation

can be rewritten according to a real formulation:

$$\delta_{mk}(t) = A_m \cos(d_m k \Delta \vartheta + \vartheta_m) \cos(\omega_m t + \phi_m) \tag{2}$$

The time varying term is common to all the points considered, while the angle varying term represents the amplitude of the displacement of each point, thus the eigenvector can be written as:

$$\mathbf{v}_m = [A_m \cos(d_m \Delta \vartheta + \vartheta_m), A_m \cos(2 d_m \Delta \vartheta + \vartheta_m), \ldots, A_m \cos(N_B d_m \Delta \vartheta + \vartheta_m)]^T \tag{3}$$

where each sector has the index $k = 1, 2, \ldots, N_B$. When many points are considered in each sector, instead of just a single one, a point index p has to be introduced, for example $p = 1, 2, \ldots, 8$ in Fig. 2 (b). The displacement δ_{mk} still follows the same dependency as in Eq. 2 but the amplitude A_{mp} is different from point to point within a single sector, thus the modal eigenvector is:

$$\mathbf{v}_m = [\ldots, A_{mp} \cos(d_m k \Delta \vartheta + \vartheta_m), \ldots]^T \tag{4}$$

The availability of the NND associated with each natural mode is essential to avoid resonances. Particular operational conditions can excite only modes with a specific NND value, otherwise the resonance is not full though the natural and the load frequencies are equal or at least similar. This implies the need for an accurate evaluation of the NND regarding the experimental tests. If the NND is the only shape information to be extracted from the mode, the most simple approach is to measure the vibrational speed at N_B points with the same location on each wheel sector. This kind of test determines the NND of all the modes within an investigated frequency range, and suffices for plotting the SAFE diagram of the wheel [25, 26]. As d_m is the angular frequency of Eq. 2, it can be uniquely determined by computing a Discrete Fourier Transform (DFT) in the angular domain and then finding d_m as the harmonic component with the maximum amplitude. When dealing with high NND ($d_m \to d_{\max}$), the DFT procedure is needed since the experimental results are not easily interpreted with a single excitation source, while conversely, the low NND modes are easily characterised. However, the NND is not the only relevant information regarding the modes. If a more detailed shape description is needed (e.g. to estimate the blade deformation) multiple measurement points are required for each sector. Indeed, just measuring one point on each sector does not distinguish between different modes with the same NND, for example in terms of the MAC matrix as discussed below, because there is not a sufficient number of degrees of freedom to evaluate the complete modal shapes. Both approaches, single point per sector for the SAFE diagram, and multiple points per sector for the MAC matrix, were performed on two different types of bladed wheels: unshrouded and shrouded.

3.2 MAC matrix

One of the most commonly used tools for evaluating the experimental modal analysis results is the Modal Assurance Criterion (MAC) matrix [37–40]. Two sets of modal eigenvectors are compared to assess their consistency, but with no consideration of the frequencies. The MAC is a matrix, usually square, whose size is the number of natural modes compared from the two different sets. This comparison is typically between experimentally measured and FE simulated modes. The generic element of the matrix represents the result of the scalar product between a couple of eigenvectors being compared:

$$M_{rs} = \frac{(\mathbf{v}_r^{\mathrm{T}} \mathbf{v}_s)^2}{(\mathbf{v}_r^{\mathrm{T}} \mathbf{v}_r)(\mathbf{v}_s^{\mathrm{T}} \mathbf{v}_s)} \tag{5}$$

where M_{rs} is the comparison quantifier between the r-th mode from the first set (experimental) and the s-th mode from the second set (numerical). The orthogonality of eigenvectors with respect to the mass matrix can be theoretically proved [41]. This means that the scalar product between two eigenvectors, associated with different modes, returns zero if the mass matrix is used as product weighting, while the scalar product between two eigenvectors associated with the same mode returns unity. The MAC matrix can therefore quantify the quality of the test results: if the diagonal terms are close to unity and the out-of-diagonal terms are close to zero, a good correlation between the compared mode sets is proved. The MAC matrix can also be used as a tool to plan the placing of the measurement points by means of the *auto*-MAC matrix. If an FE model is available, different potential measurement positions can be considered and then the corresponding eigenvectors extracted. The auto-MAC matrix is computed by comparing the FE modes with each other and thus obtaining information on the quality of the chosen points. A good location pattern returns zero values (or almost zero) in the MAC matrix out-of-diagonal terms, while any ineffective location returns high out-of-diagonal terms. When an experimental test and the related FE results are compared, if the real representation is applied, the FE modes are necessarily in the form of Eq. 3, and the term ϑ_m of the FE eigenvectors is supposedly a free parameter. In the present work, ϑ_m was chosen as the phase producing the most constructive combination between the modes, i.e. the maximizing value for M_{rs} for each r, s combination, both for diagonal and out-of-diagonal terms. Conversely, if the complex modal representation is followed, and the complex MAC is calculated accordingly, a unique real value is obtained for M_{rs} regardless of the choice of any ϑ_m [17]. The null or almost zero M_{rs}, for $r \neq s$, is theoretically valid only if an adequate number of degrees of freedom is considered for the modal representation. If only a few measurement points are taken into account, a comparison between any two different eigenvectors can be misleading since a high MAC value can erroneously result. On the other hand, if the mass matrix is not available, for example in experimental tests, the scalar product between the eigenvectors

does not return zero even if different modes are combined. The modal shapes can be found by analysing the eigenvectors of the matrix $E = W^{-1}K$, where K represents the stiffness symmetric matrix, and W represents the diagonal mass matrix. If the diagonal elements of W are equal to each other, $W^{-1}K$ is a symmetric matrix, which always has orthogonal eigenvectors, and thus $M_{rs} = 0$ if r-th and s-th are distinct modes. On the other hand, if the diagonal elements of W are significantly not equal, the out-of-diagonal elements of the MAC matrix can be greater than zero though comparing distinct modes. Thus it follows that the more different from unity the ratios of the mass matrix diagonal terms are, the higher the MAC matrix out-of-diagonal elements. In addition, deformable bodies have an infinite number of degrees of freedom, while an eigenvector defined in an experimental framework has a finite number of measurement points, hence certain modes cannot be fully represented and some cannot be completely distinguished. Finally, when dealing with experimental data, the measurement precision obviously introduces another source of error. Among all these sources of high out-of-diagonal MAC values, the unevenness of the mass matrix can be eliminated by choosing a suitable pattern of the measurement points, each representing an equal amount of mass. When symmetric structures are investigated, after picking the corresponding points on each repeated sector, the same amount of mass is obviously associated with each point. Similarly, if several points are measured for every sector, instead of just one, different eigenvectors still have a low MAC value. This can be proved by considering the multi-point eigenvector, Eq. 4, as a combination of single point sub-eigenvectors. Each sub-eigenvector couple, as extracted by the two modes to be compared, returns almost zero out-of-diagonal MAC values. When these sub-eigenvectors are finally combined in the full eigenvectors, the scalar product still is the sum of the sub-eigenvector scalar products, thus again returning almost zero out-of-diagonal MAC values.

## 4 Experimental results and FE validations

In the performed tests the excitation was applied at a single point with an electrodynamic shaker. The aim of this research was to recognize the shape of the modes, instead of focusing on detecting and separating the double modes, since they appear as the same point in the SAFE diagram. However, to identify the double modes of the wheel, the proposed measuring set up can still be useful, but at least two independent load inputs need to be applied at separate points of the structure [36]. The experimental modal analyses reported here are distinguished as *single*-point and *multi*-point for each sector. The first approach is sufficient for the determination of the modal NND, which is indeed the SAFE diagram horizontal coordinate, while the second is more general and provides a potentially deeper spatial description of the modal shapes. The first component was an unshrouded bladed wheel with splitter blades. An

initial single-point analysis was performed just considering main blade tips. The test was then repeated considering both main and splitter blades, in order to introduce the particular property of this kind of wheel. The second tested element was a shrouded bladed wheel, with one blade per sector. Here a multi-point analysis was performed, and a sub-eigenvector was extracted from the full one to represent the single-point analysis and to derive the SAFE diagram. The effectiveness of the multi-point analysis, to identify the shapes of different modes sharing the same NND, was demonstrated by comparison with the single-point analysis.

4.1 Single-point analysis

The first article tested was an unshrouded centrifugal compressor bladed wheel with 11 sectors. Each sector featured a main blade and a splitter blade, i.e. a smaller blade that reduces the rotor vane section at the outer diameter. Since the component has 11 symmetric sectors, the maximum NND is $d_{max} = 5$. This is explained by the fact that only 11 homologous points can be found on the wheel, thus it is not possible to have a frequency greater than 5 as a consequence of the Nyquist-Shannon sampling theorem [42]. In any case, the combination between the excitation and the modal shape depends on the displacement sign distribution of the load application points. The points at the outer diameter experience a cyclic load determined by the outlet flow of the machine, and here 22 blades are present on the circumference hoop: 11 main blades plus 11 splitter blades. The NND obtained by an FE simulation with a sector model, imposing the cyclic symmetric boundary conditions, correctly represents the actual scenario only if the main blade and the splitter blade have the same phase in each sector. On the other hand, if they are out of phase, the number of sign reversals along the circumference hoop will switch from $2\overline{d_m}$ ($\overline{d_m}$ being the value given by the cyclic FE model) to $2d_{max} - 2\overline{d_m}$. A proof of this statement can be found in the Appendix. This phenomenon was experimentally verified by performing two different tests: only one point on the main blade tip was initially measured, and then two points per sector were measured, one at the main blade edge and the other at the splitter blade edge. The measurement point locations and the SAFE diagram results are reported in Figs. 5 and 6 for one point per sector and one point per blade respectively, where the results are normalized with respect to the first experimental natural frequency ("Exp." represents the experimental tests and "FE" the FE model results). When only one point per sector is measured, the results can be directly compared with the FE analysis in terms of frequency and NND. Figure 5 (b) shows the SAFE diagram of the modes obtained in the first test and a clear correlation with the FE results can be observed. All the 18 modes within the range of interest were successfully detected and the relative differences, with respect to the numerical results, were found to be lower than 1%. The

frequency ranges with a high density of modes were also successfully investigated. The measurement time was set

at 0.8 s in order to have an adequate frequency resolution of 1.25 Hz. This value was considered to be sufficiently

small compared to the detected modal frequencies, which were in the order of kHz for the range investigated.

In this specific test, two modes were detected at incorrect number of nodal diameters, horizontally shifted in the

SAFE diagram to other modes with very similar frequency values. These modes were found to show a DFT with

two peaks, but the one at the expected NND, though relevant, was not the maximum. This issue could be better

investigated with two independent load inputs, to verify if the tested wheel actually has a slightly different dynamics

from the FE model prediction.

(a)   (b)
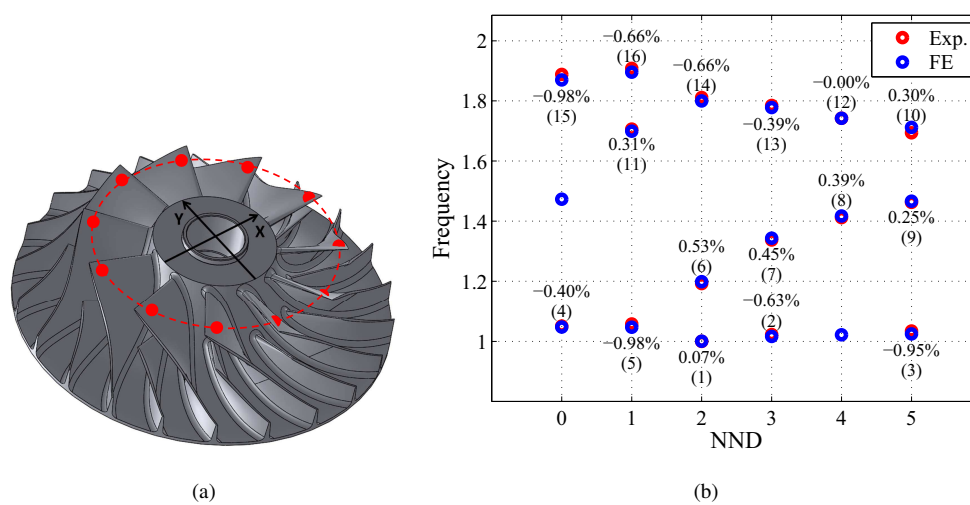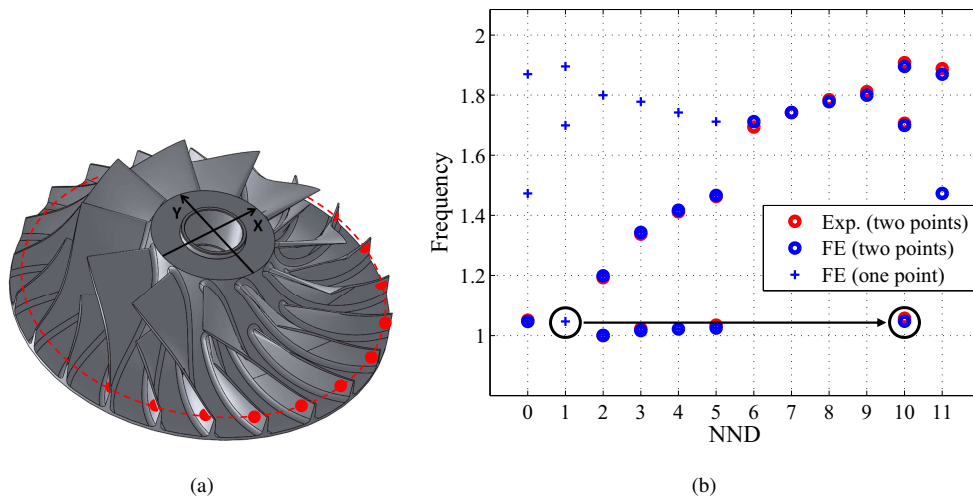
Fig. 5 One point for each sector: (a) measurement locations, (b) SAFE diagram to compare test and FE results.

The test was then repeated with the measurement points at the outlet edge of the blades, Fig. 6 (a), by measuring both

the main and the splitter blades vibrational responses. The obtained eigenvectors were preliminarily split into two

parts to separate the main blades from the splitter blades, which enabled the results of the first test to be validated.

The full eigenvector was then considered, containing all 22 points, and the actual number of displacement sign

reversals along the circumferential hoop direction was analysed. Figure 6 (b) shows the SAFE diagram obtained in

this situation compared to the FE model which also considers the entire set of measurement points. The NND of

some modes switched from $\overline{d_m}$ to $d_{max} - \overline{d_m}$ according to the aforementioned analysis.

### 4.2 Multi-point analysis results

The second component tested was a shrouded bladed wheel with 15 sectors and without the splitter blades. The

test was performed by measuring eight points for each sector, on the blade inlet edge, as shown in Fig. 7 (a), with

(a)   (b)

**Fig. 6** Two points for each sector: (a) measurement locations, (b) extended SAFE diagram.

reference to Fig. 2 (b) regarding the test set up. The total number of measurement points was 120, and the overall testing time was approximately 2 hours, which is just 1 minute for each measurement. For the points along the edge of each blade, the placing was performed without returning to the rest position. In order to determine the main shape parameter, i.e. the number of nodal diameters, only the fifth point in the central region of each blade was considered, as denoted by the dashed line in Fig. 7 (a). The experimental results were then compared to the FE analysis in terms of SAFE diagram coordinates, Fig. 7 (b). A full agreement between the experimental and numerical NND was found, and the maximum difference in modal frequencies was still quite small (approx. 2%) for all the 13 modes in the frequency range investigated.

(a)   (b)
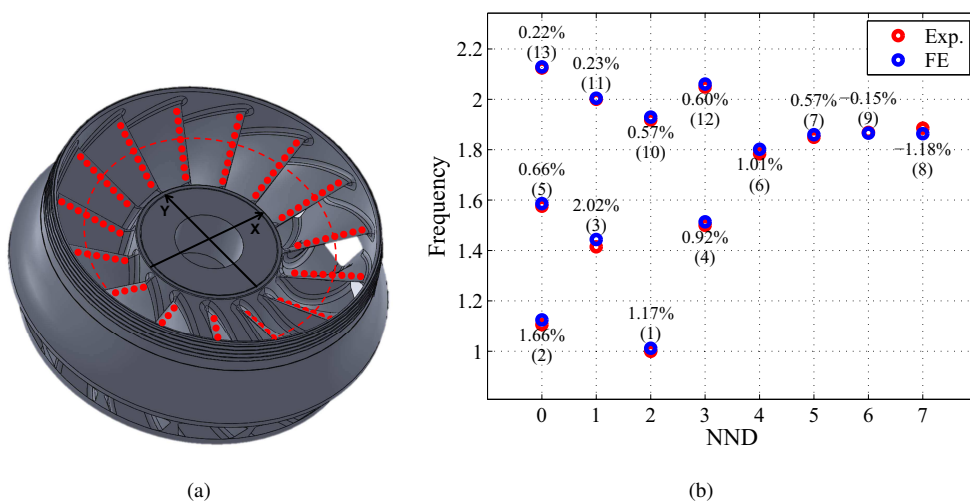
Fig. 7 Multiple point test on a shrouded bladed wheel: (a) measurement locations, (b) SAFE diagram.

In order to prove the enhancement effect on the modal characterization induced by the large number of measurement

points, the MAC matrix was computed for the sub-eigenvectors and for the full eigenvectors. The measurements

at the central point of each blade were extracted from the full eigenvector for the single-point approach. Figure

8 (a) shows the computed MAC matrix for this virtual single point test, showing several nonzero out-of-diagonal

values (e.g. the mode combinations 1 to 10 and 2 to 5). The white numbers on the MAC matrix plot are the NNDs

computed for each mode. All the out-of-diagonal nonzero terms corresponded to those modes sharing the same

NND, thus proving that for these cases the single point test does not distinguish between different modes. The MAC

matrix computation was then repeated for the full eigenvectors, Fig. 8 (b), showing a significant reduction in the

correlation values of the mode couples 2-5 and 1-10.
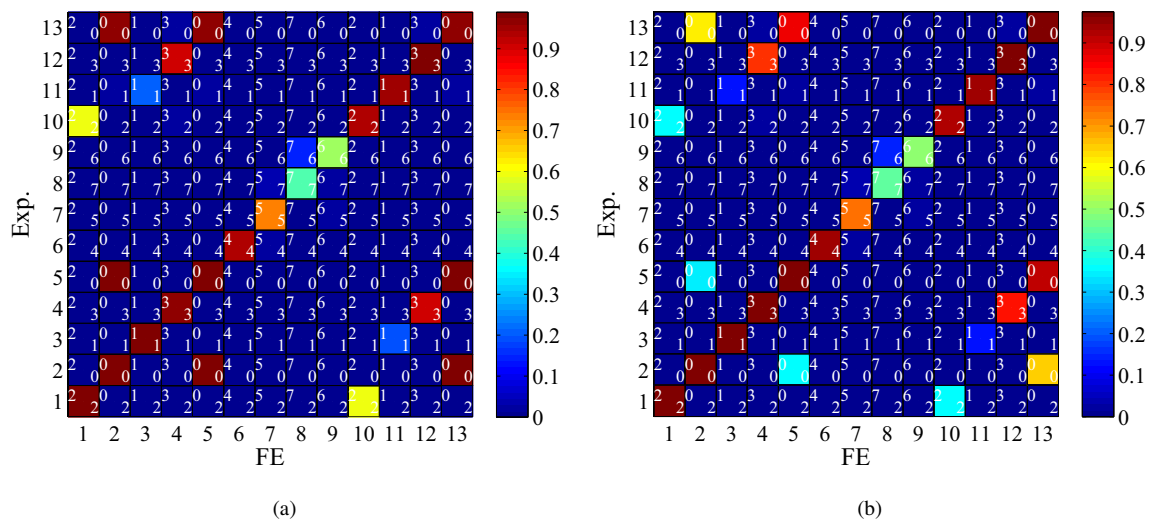
Fig. 8 MAC matrices for comparison between the experimental and the numerical results: (a) single point per sector, (b) multiple point
per sector.

Figure 9 compares modes 2 and 5, which both have $d_m = 0$. This comparison highlights the difference between

these two modes in terms of how the blade is bent, which can only be noticed if several points on each blade are

measured. More specifically, the second experimental modal shape is compared to the fifth numerical mode. The

MAC matrix elements $M_{2,5}$ and $M_{5,2}$ decreased with respect to the values previously obtained with the single-point

test. All the other nonzero out-of-diagonal terms are also reduced, though to a lesser extent. However, the high

frequency modes have more complicated modal shapes which is why an even larger number of measurement points

would be needed to identify all of them. The diagonal values of the MAC matrices reported in Figs. 8 (a) and (b) are

very close to 1, except for the modes 8 and 9. In fact, these two modes feature high NNDs, close to the maximum:

NND = 7 and NND = 6, respectively, with $d_{max} = 7$. A more complex test set up, with at least two excitation points,

rather than just one, would be needed to excite them for this experimental characterization.
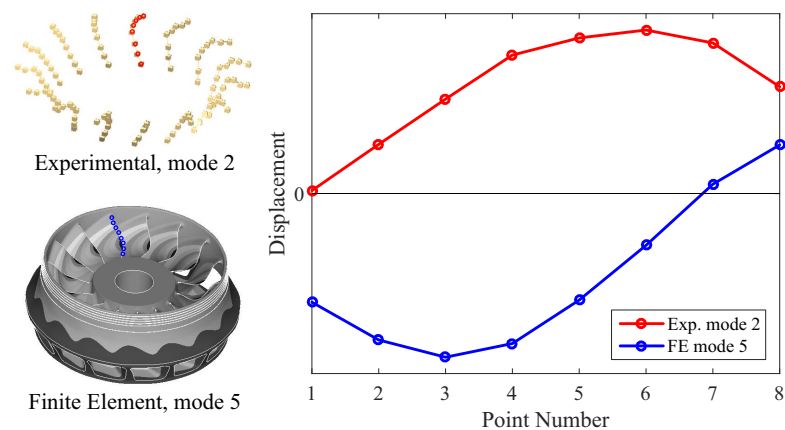
Fig. 9 Comparison between two distinct modes, experimental and FE simulated, sharing the same NND.

5 Conclusions

This paper has presented an experimental set up to perform a fully automated modal analysis of mechanical components. This procedure was then applied to centrifugal compressor bladed wheels. An anthropomorphic robotic arm was used to point a Laser Doppler Vibrometer sensor on selected measurement locations to obtain fast and, more importantly, accurate positioning and orientation, even for these highly three-dimensional articles. The characteristics of the investigated bladed wheel types have been discussed and the results of different tests presented and compared to FE modelling. The tests with a single point for each blade characterize the modes sufficiently when only the number of nodal diameters is required (as for the SAFE diagram) and successful comparative results were obtained with respect to the FE prediction. The particular feature of the splitter blade wheels was also analysed. By having one point for each splitter blade, i.e. two points for each sector, an extended SAFE diagram was newly proposed, where the maximum number of nodal diameters follows the load input either at the inner or at the outer wheel circle. Finally, by measuring a certain number of points for each wheel sector, the experimental modes were better described, providing an improvement in the MAC matrix results and an increased resolution of the vibrational shapes. This modal shape enhanced representation could be exploited to expand the SAFE diagram and provide a more sophisticated definition for the modal-to-load shape matching.

References

1. S. Houde, R. Fraser, G.D. Ciocan, and C. Deschênes. Part 1 - experimental study of the pressure fluctuations on propeller turbine runner blades during steady-state operation. In *Proceedings of the 26th IAHR Symposium on Hydraulic Machinery and Systems*, pages 1–14, 2012.

2. M. Sunar and B.O. Al-Bedoor. Vibration Measurement of Rotating Blades Using a Root Embedded PZT Sensor. *Shock and Vibration*, 15:517–541, 2008.

3. M.N. Helfrick, P. Pingle, C. Niezrecki, and P. Avitabile. Optical non-contacting vibration measurement of rotating turbine blades. In *Proceedings of the IMAC-XXVII*, pages 1–5, 2009.

4. J. Baqersad, T. Lundstrom, C. Niezrecki, and P. Avitabile. Monitoring the Dynamics of an Operating Helicopter Rotor Using 3D Digital Stereophotogrammetry. In *Proceedings of the 11th International Conference on Recent Advances in Structural Dynamics (RASD)*, pages 1–11, 2013.

5. S. Zucca and B.I. Epureanu. Detection of a Blade Crack in Bladed Disks: Methodology and Validation. In *26th International Conference on Noise and Vibration Engineering, ISMA 2014, Including the 5th International Conference on Uncertainty in Structural Dynamics, USD 2014*, pages 2851–2866, 2014. ISBN: 978-907380291-9.

6. A.J. Oberholster and P.S. Heyns. Online condition monitoring of axial-flow turbomachinery blades using rotor-axial eulerian laser doppler vibrometry. *Mechanical Systems and Signal Processing*, 23(5):1634–1643, 2009.

7. P Neri and B. Peeters. Non-harmonic fourier analysis for bladed wheels damage detection. *Journal of Sound and Vibration*, 356:181–194, 2015.

8. K. Motte, W. Weijtjens, C. Devriendt, and P. Guillaume. Operational modal analysis in the presence of harmonic excitations: A review. In *Conference Proceedings of the Society for Experimental Mechanics Series*, volume 2, pages 379–395, 2015.

9. F. Trebuňa and M. Hagara. Experimental modal analysis performed by high-speed digital image correlation system. *Measurement*, 50:78–85, 2014.

10. Y. Bidaut and U. Baumann. Identification of eigenmodes and Determination of the Dynamical Behaviour of Open Impellers. In *Proceedings of ASME Turbo Expo*, volume 7 of *PARTS A AND B*, pages 1063–1073, 2012. GT2012-68182.

11. M.P. Castanier and C. Pierre. Modeling and Analysis of Mistuned Bladed Disk Vibration: Status and Emerging Directions. *Journal of Propulsion and Power*, 22(2):384–396, 2006.

12. D. Di Maio and D.J. Ewins. Applications of continuous tracking sldv measurement methods to axially symmetric rotating structures using different excitation methods. *Mechanical Systems and Signal Processing*, 24:3013–3036, 2010.

13. S. Zucca, D. Di Maio, and D.J. Ewins. Measuring the performance of underplatform dampers for turbine blades by rotating laser doppler vibrometer. *Mechanical Systems and Signal Processing*, 32:269–281, 2012.

14. B.J. Halkon and S.J. Rothberg. Vibration measurements using continuous scanning laser vibrometry: Advanced aspects in rotor applications. *Mechanical Systems and Signal Processing*, 20:1286–1299, 2006.

15. P. Giuliani, D. Di Maio, C.W. Schwingshackl, M. Martarelli, and D.J. Ewins. Six degrees of freedom measurement with continuous scanning laser doppler vibrometer. *Mechanical Systems and Signal Processing*, 38:367–383, 2013.

16. M. Martarelli and P. Castellini. Performance analysis of continuous tracking laser doppler vibrometry applied to rotating structures in coast-down. *Measurement Science and Technology*, 23:1–12, 2012.

17. L. Bertini, B.D. Monelli, P. Neri, C. Santus, and A. Guglielmo. Robot assisted modal analysis on a stationary bladed wheel. In *ASME 2014 12th Biennial Conference on Engineering Systems Design and Analysis, ESDA 2014*, pages 1–8, 2014.

18. Polytec GmbH. RoboVib Structural Test Station. http://www.polytec.com/us/products/vibration-sensors/scanning-vibrometers/robovib-structural-test-station/.

19. W.-H. Jeon. A numerical Study on the Acoustic Characteristics of a Centrifugal Impeller with a Splitter. *GESTS Int'l Trans. Computer Science and Engineering*, 20(1):17–28, 2005.

20. M. Gölcü, Y. Pancar, and Y. Sekmen. Energy saving in a deep well pump with splitter blade. *Source of the Document Energy Conversion and Management*, 47(5):638–651, 2006.

21. M. Gölcü, N. Usta, and Y. Pancar. Effects of splitter blades on deep well pump performance. *Journal of Energy Resources Technology, Transactions of the ASME*, 129(3):169–176, 2007.

22. G. Kergourlay, M. Younsi, F. Bakir, and R. Rey. Influence of splitter blades on the flow field of a centrifugal pump: Test-analysis comparison. *International Journal of Rotating Machinery*, 2007(85024):1–13, 2007.

23. N.Y. Sharma and K.V. Karanth. Numerical analysis of a centrifugal fan for improved performance using splitter vanes. *World Academy of Science, Engineering and Technology*, 60:453–459, 2011. ISSN: 2010376X.

24. A. Kammerer and R.S. Abhari. Experimental Study on Impeller Blade Vibration During Resonance - Part I: Blade Vibration Due to Inlet Flow Distortion. *Journal of Engineering for Gas Turbines and Power*, 131(2):art. no. 022508, 2009.

25. H.P. Bloch and M. Singh. *Steam Turbines: Design, Applications and Re-Rating*. McGraw-Hill, 2nd edition, 2008.

26. L. Bertini, P. Neri, C. Santus, A. Guglielmo, and G. Mariotti. Analytical investigation of the safe diagram for bladed wheels, numerical and experimental validation. *Journal of Sound and Vibration*, 333(19):4771–4788, 2014.

27. T. Berruti, C.M. Firrone, and M.M. Gola. A test rig for noncontact traveling wave excitation of a bladed disk with underplatform dampers. *Journal of Engineering for Gas Turbines and Power*, 133(3):032502, 2011.

28. P. Castellini, G.M. Revel, and L. Scalise. Measurement of vibrational modal parameters using laser pulse excitation techniques. *Measurement*, 35:163–179, 2004.

29. S. Vanlanduit, F. Daerden, and P. Guillaume. Experimental modal testing using pressurized air excitation. *Journal of Sound and Vibration*, 299:83–98, 2007.

30. R. Farshidi, D. Trieu, S.S. Park, and T. Freiheit. Non-contact experimental modal analysis using air excitation and a microphone array. *Measurement*, 43:755–765, 2010.

31. L. Bertini, P. Neri, and C. Santus. Design and optimization of a compact high-frequency electromagnetic shaker. In *Proceedings of 11th International Conference on Engineering Vibration*, pages 1–9, 2015.

32. P. Neri. Excitation device for high frequency vibration analysis: design and test results. *Experimental Techniques*, 2015. Submitted.

33. P. Vargiu, C.M. Firrone, S. Zucca, and M.M. Gola. A reduced order model based on sector mistuning for the dynamic analysis of mistuned bladed disks. *International Journal of Mechanical Sciences*, 53(8):639–646, 2011.

34. C. Jung, A. Saito, and B.I. Epureanu. Detection of cracks in mistuned bladed disks using reduced-order models and vibration data. *Journal of Vibration and Acoustics*, 134(6):art. no. 61010, 2012.

35. O. Marinescu, B.I. Epureanu, and M. Banu. Reduced order models of mistuned cracked bladed disks. *Journal of Vibration and Acoustics*, 133(5):art. no. 051014, 2011.

36. D.J. Ewins. *Modal Testing, Theory, Practice and Application*. Research Studies Press Ltd - Wiley, 2nd edition, 2000. ISBN 978-0863802188.

37. L. Rignér. Modal assurance criteria value for two orthogonal modal vectors. In *Proceedings of the International Modal Analysis Conference - IMAC 2*, pages 1320–1325, 1998.

38. R.J. Allemang. The modal assurance criterion - Twenty years of use and abuse. *Sound and Vibration*, 37(8):14–21, 2003.

39. P. Vacher, B. Jacquier, and A. Bucharles. Extensions of the MAC criterion to complex modes. In *Proceedings ISMA2010-USD2010*, pages 2713–2726, 2010.

40. M. Pástor, M. Binda, and T. Harčarik. Modal Assurance Criterion. In *MMaMS 2012*, volume 48 of *Procedia Engineering*, pages 543–548, 2012.

41. L. Meirovitch. *Fundamentals of Vibrations*. Waveland Press, Inc., 2001. ISBN 978-1-57766-691-2.

42. Robert J. Marks II. *Introduction to Shannon Sampling and Interpolation Theory*. Springer-Verlag, New York, 1991. ISBN 3-540-97391-5.

A NND shift for the splitter blade wheels

The splitter blade wheels have two blades for each sector and a total of $2N_S$ blades, where N_S is the number of sectors. If the vibrational relative displacement between the main and the splitter blades is out of phase, the number of sign reversals along the circumference hoop changes from $2\overline{d_m}$ to $2d_{\max} - 2\overline{d_m}$. Regarding the generic m-th mode, $\overline{d_m}$ refers just to one group of blades, either main or splitter, and $\overline{d_m}$ is also coincident to the NND calculated by an FE modal analysis under cyclic symmetric boundary conditions. Therefore, for any generic mode, after considering all the blades and with splitter and main blades out-of-phase, the NND is:

$$d_m = d_{\max} - \overline{d_m} \tag{6}$$

where $d_{\max} = \lfloor N_B/2 \rfloor$ and with $N_B/2 = N_S$, it follows that $d_{\max} = N_S$. Equation 6 can be demonstrated by referring to Fig. 10. The main blades are represented with a red circle, the splitter blades are represented with a blue circle, and the N_S sectors are marked with a black dashed line. With the out-of-phase vibration of the main and the splitter blades, it is then possible to draw $\overline{d_m}$ diameters by splitting the main blades into groups with the same sign, red lines in Fig. 10 (a), and $\overline{d_m}$ diameters for the splitter blades, blue lines in Fig. 10 (a), hence the total number of diameters drawn equals $2\overline{d_m}$. For a graphical representation, the red circular sectors highlight how the blades are grouped by the nodal diameters corresponding to the main blades. If $\overline{d_m} = 0$, all the main blades have the same sign, all the splitter blades have the opposite sign, thus for this specific case, the total number of sign reversals equals N_B which is the maximum possible number. On the other hand, if $\overline{d_m} \neq 0$, the number of sign reversals is lower and equals $N_B - N'$, where N' is the number of sign continuities. Along the circumference hoop, all the main blades have the same sign until a nodal diameter is met. Since the splitter blades are out of phase with respect to the main, a sign reversal is found by moving from every main blade to an adjacent splitter blade. When a nodal diameter is crossed, the main blades change their sign. In this situation a sign reversal may or may not occur depending on the blade position with respect to the nodal diameter considered. Any diameter splits two couples of blades (each couple consisting of one main and one splitter blade). The blades of each couple may belong to the same sector or to different sectors. If the blades of the couple belong to the same sector, they are out of phase, thus a sign reversal is found by crossing the nodal diameter. On the other hand, if the nodal diameter splits the blade belonging to sector S_1 and the blade belonging to sector S_2, no sign reversal is found, Fig. 10 (b). The main blades belonging to those two sectors necessarily have different signs, since they are divided by a nodal diameter. The splitter blade of sector S_1 also has a different sign with respect to the main blade of its own sector. This implies that the splitter blade of sector S_1 must have the same sign as the main blade of sector S_2, thus no sign reversal is found by crossing the nodal diameter. At this point, a distinction between even and odd N_S must be considered. When N_S is even, both the couples split by a nodal diameter have the same behaviour in terms of sign reversals. Indeed, the nodal diameter divides the wheel in two portions of π, while each sector angular width is $\vartheta_S = 2\pi/N_S = \pi/A$, A being an integer since N_S is even. Therefore, in each portion determined by the nodal diameter, the number of sectors equals $\pi/\vartheta_S = A$. Consequently, if one of the couples split by the nodal diameter contains two blades of the same sector, the second couple also contains two blades of the same sector, otherwise both the couples would contain blades belonging to different sectors. Each nodal diameter corresponding to the main blades, the red lines in Fig. 10 (a), has its counterpart corresponding to the splitter blades, the blue lines in Fig. 10 (a). This counterpart is shifted by π/N_S (half sector) with respect to the nodal diameter corresponding to the main blades. This implies that if the nodal diameter corresponding to one of the blade series causes the sign reversal, its counterpart does the opposite and vice versa. Consequently, the number of nodal diameters causing a sign reversal equals $\overline{d_m}$, which is half the total number of nodal diameters drawn. Each nodal diameter can determine two sign reversals, thus $N'' = 2\overline{d_m}$ where N'' is

the number of sign reversals crossing a nodal diameter. Indeed, the sign reversals are always found by moving from a main blade to a splitter blade except when a nodal diameter splitting two blades of different sectors is crossed. When N_S is odd, if one of the two couples split by a nodal diameter contains blades belonging to the same sector, then the second couple necessarily contains blades belonging to different sectors. It follows that every nodal diameter has one sign reversal at one end and no sign reversal at the other. Since the total NND is $2\overline{d_m}$ and each nodal diameter determines only one sign reversal, it is possible to state again that $N'' = 2\overline{d_m}$. Consequently, it has been proven that either with N_S odd or even, $N'' = 2\overline{d_m}$. Obviously, the total number of crossings is $4\overline{d_m} = N' + N''$, hence it follows that $N' = 4\overline{d_m} - N'' = 2\overline{d_m}$, and the total number of sign reversals is $N_B - N' = N_B - 2\overline{d_m}$. Since the actual NND, considering the two series of blades, equals half the number of sign reversals, it holds that $d_m = N_B/2 - \overline{d_m} = d_{\max} - \overline{d_m}$, as claimed. In conclusion, since in each sector the blades can only vibrate in phase or out of phase (if dumping is negligible or not taken into account), it is possible to state that the actual NND equals $\overline{d_m}$ if the main and the splitter blades are in phase, while it is $d_{\max} - \overline{d_m}$ if they vibrate out of phase.
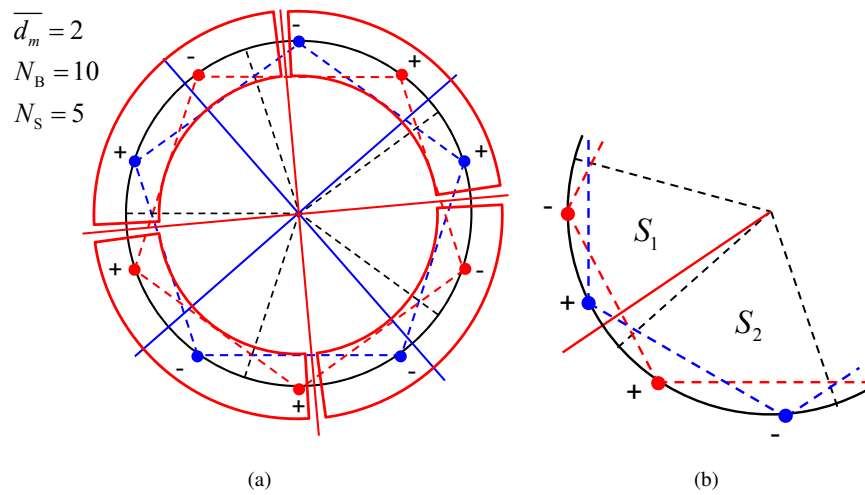
Fig. 10 (a) Sign reversals of a rotor with splitter blades, (b) sign continuity at a nodal diameter crossing.